Final Report

Gas/Surface Interaction Study Applied to Si-based Materials Used in Driven Micro- and Nano-scale devices

Author: Prof. Sergey Borisov
Institution: Ural State University
              General & Molecular Physics Department
              51 Lenin Ave
              Ekaterinburg, Russia

Report Documentation Page		Form Approved OMB No. 0704-0188

Public reporting burden for the collection of information is estimated to average 1 hour per response, including the time for reviewing instructions, searching existing data sources, gathering and maintaining the data needed, and completing and reviewing the collection of information. Send comments regarding this burden estimate or any other aspect of this collection of information, including suggestions for reducing this burden, to Washington Headquarters Services, Directorate for Information Operations and Reports, 1215 Jefferson Davis Highway, Suite 1204, Arlington VA 22202-4302. Respondents should be aware that notwithstanding any other provision of law, no person shall be subject to a penalty for failing to comply with a collection of information if it does not display a currently valid OMB control number.

1. REPORT DATE **2010**	2. REPORT TYPE	3. DATES COVERED **00-00-2010 to 00-00-2010**

4. TITLE AND SUBTITLE **Gas/Surface Interaction Study Applied to Si-based Materials Used in Driven Micro- and Nano-scale devices**		5a. CONTRACT NUMBER
		5b. GRANT NUMBER
		5c. PROGRAM ELEMENT NUMBER
6. AUTHOR(S)		5d. PROJECT NUMBER
		5e. TASK NUMBER
		5f. WORK UNIT NUMBER
7. PERFORMING ORGANIZATION NAME(S) AND ADDRESS(ES) **Ural State University,General & Molecular Physics Ddepartment,51 lenin Ave,Ekaterinburg, Russia,**		8. PERFORMING ORGANIZATION REPORT NUMBER
9. SPONSORING/MONITORING AGENCY NAME(S) AND ADDRESS(ES) **EOARD, , , , ,**		10. SPONSOR/MONITOR'S ACRONYM(S)
		11. SPONSOR/MONITOR'S REPORT NUMBER(S)

12. DISTRIBUTION/AVAILABILITY STATEMENT
Approved for public release; distribution unlimited

13. SUPPLEMENTARY NOTES
DTIC Submission - CRDF 069002 Per EOARD email subject line dated dated 26 July 2010.

14. ABSTRACT

15. SUBJECT TERMS

16. SECURITY CLASSIFICATION OF:			17. LIMITATION OF ABSTRACT	18. NUMBER OF PAGES	19a. NAME OF RESPONSIBLE PERSON
a. REPORT **unclassified**	b. ABSTRACT **unclassified**	c. THIS PAGE **unclassified**	**Public Release**	**25**	

Standard Form 298 (Rev. 8-98)
Prescribed by ANSI Std Z39-18

Table of Contents

YEAR 1:

Task 1: Development of experimental approaches and their adaptation for gas/surface systems declared in the project.

A hot filament method is used to study the heat transfer between tungsten surface and hollow cathode glow discharge plasmas in argon and CO_2. The dependence of the electric power supplied to a tungsten wire on the discharge current is determined for argon and carbon dioxide in the temperature range between 1000K and 1700 K. A difference in heat transfer at the tungsten wire surface is found between experiments on argon and carbon dioxide. The difference is attributed to heterogeneous recombination in CO_2 plasma.

It is hardly possible to enumerate all applied and fundamental issues related to energy transfer across plasma–solid interfaces. Problems of this kind arise in areas ranging from aerothermodynamics to plasma enhanced chemical vapor deposition, sputtering, and etching technologies. Therefore, research on this subject is important from both theoretical and practical perspectives. Of particular importance are further experimental studies using various techniques with a view to improving theoretical models of plasma–surface interaction.

The choice of a hot filament technique, widely used in studies of heat transfer in low pressure gas–surface systems starting from Knudsen's work, has the technical advantage of simple processing control.

Tungsten is used as a filament material for the following reasons. First, tungsten is a metal with well-known electrical and thermal properties. Second, it has a high melting point of 3653 K, which makes it possible to conduct investigations in a wide temperature range. Moreover, a vast amount of data is available on heat and mass transfer at tungsten surface.

Plasma is produced in a hollow cathode glow discharge. A key advantage of this system compared to those with planar electrodes is the feasibility of a high current density through the electrode gap. Furthermore, it can be used to produce highly ionized plasmas at low gas pressures and provides good spatial resolution of glow discharge zones.

Argon and Carbon dioxide are used as working gases because they have similar molecular masses, but widely different physical and chemical properties determining the characteristics of processes that occur both in the gas phase and at gas–solid interfaces.

Figure 1.1 shows a block diagram of the experimental setup. A glow discharge chamber is mounted on insulators inside a vacuum chamber. The vacuum chamber is evacuated to a residual gas pressure on the order of 10^{-3} Pa by oil diffusion pump. The vacuum chamber is a $410 \times 430 \times 500$ mm^3 parallelepiped made of the stainless steel 12X18H10T.

The working gas is fed into the discharge chamber through an inlet duct of 3 mm in diameter via mass flow controller and evacuated through a 9 mm diameter outlet in the opposite flange. A gas flow rate set at approximately 0.2 cm^3 atm/s maintains a

discharge chamber pressure of about 1 Pa when the vacuum chamber pressure is approximately 4×10^{-2} Pa.
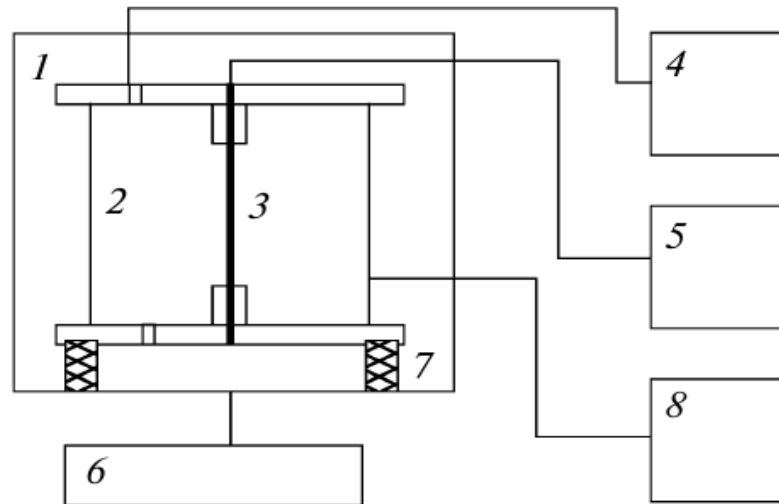

Fig. 1.1. Experimental setup: (1) vacuum chamber; (2) gas discharge chamber; (3) tungsten wire; (4) gas inlet system; (5) filament heating and temperature stabilization system; (6) evacuation system; (7) insulators; (8) discharge power supply.

Task 2: Surface preparation and diagnostics by AFM.

The surface preparation procedure depends on the task. The same is for the surface diagnostics. In particular, in experiments devoted to surface composition effect on gas flow rate in channels the system for exposure of evaporated metal or adsorbed gas is used (see below Task 7). In experiments devoted to surface chemical composition effect of heat exchange between rarefied gas and a solid body the surface preparation procedure mainly includes purification cycles based on high temperature heating (see Task 6). In both cases Auger Electron Spectroscopy as a means of surface diagnostics is used.

The problem of surface stricture effect on character on gas/surface interaction and as a result on accommodation coefficients needs attracting such means of diagnostics as Atomic Force Microscopy (AFM). In particular, for Si-based samples the following data have been obtained with the use of AFM technique (Fig.2.1, Fig2.2 and Fig.2.3).
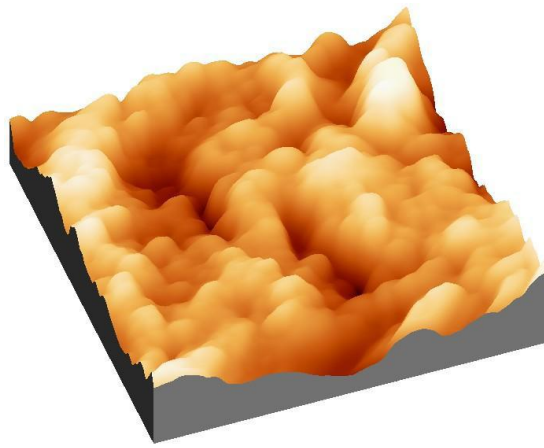
Fig.2.1. Surface structure for Si-based material according to AFM data: 3-dimensional image.
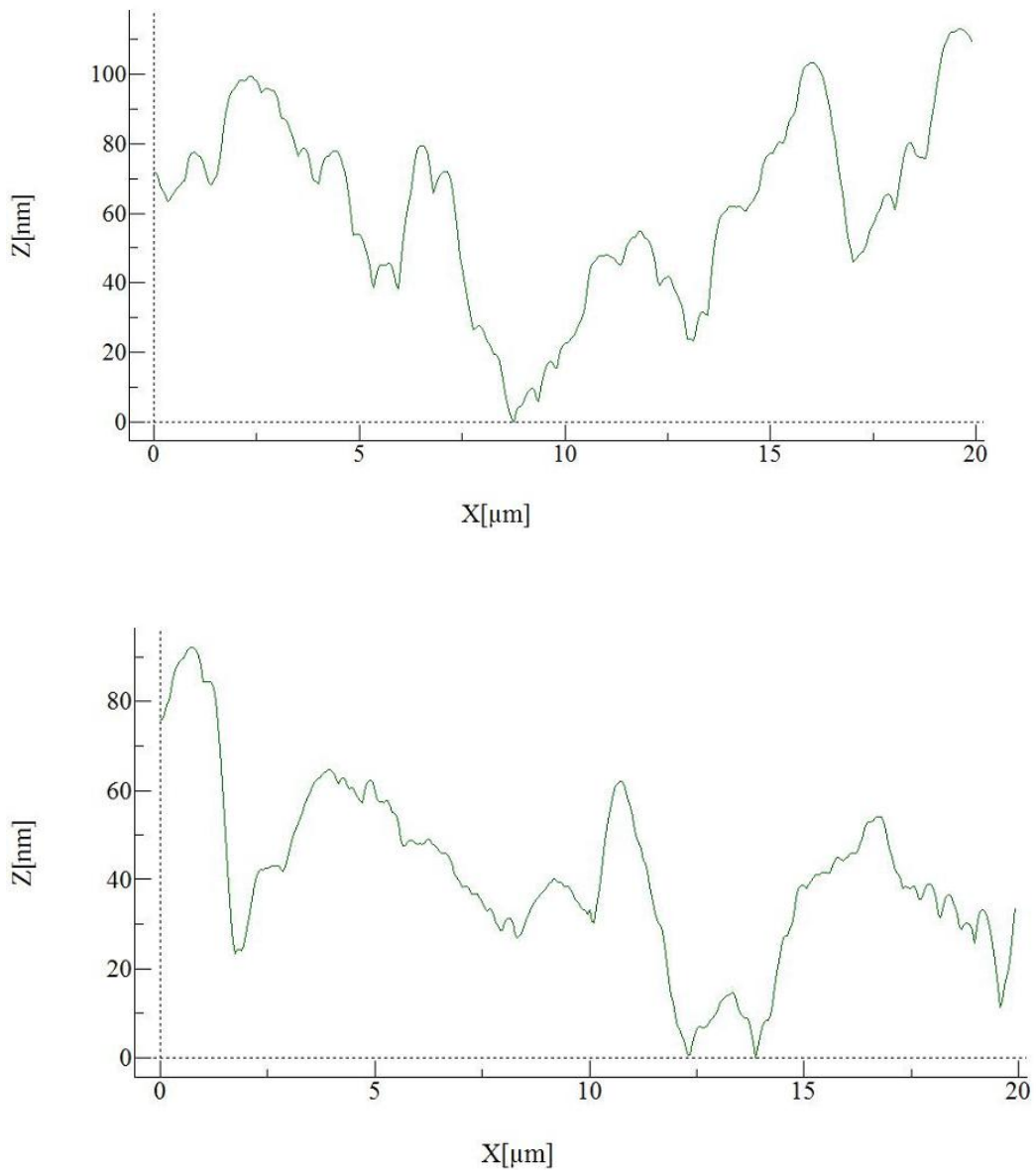

Fig.2.2. Surface structure for Si-based material according to AFM data: separate profiles along one scanning direction.
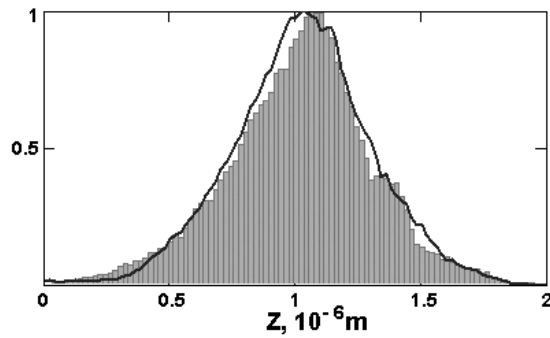
Fig2.2. Surface micro roughness distributions function for investigated sample according to AFM.

These data were used for simulation of surface structure and calculation of gas flow rate in channels (see Task 5).

TASK 3: NORMAL MOMENTUM ACCOMMODATION STUDY.

A dynamic technique for normal momentum accommodation study in a gas–surface system is developed. The method can also be used for pressure measurements and adsorption studies.

Characteristics of dynamic pressure gauges allow their application in various fields of science and engineering. For example, by measuring the frequency shift of sensor oscillations, one can measure gas adsorption on the sensor surface. Another important application of the dynamic technique is the investigation of momentum-transfer efficiency in the course of interaction of the gas and solid surface, which is generally characterized by accommodation coefficients. The values of accommodation coefficients, in particular, the normal momentum accommodation coefficient (NMAC), are mainly obtained by the molecular beam technique. Implementation of this method, however, faces significant difficulties including the problem of interpreting the results and using them to describe the processes of gas–surface interaction under weakly non equilibrium conditions.

The proposed method for NMAC measurement has significant advantages over other methods; one of advantages is the simplicity of its implementation. As for interpretation of the data obtained, it is also rather simple if some assumptions are used in a particular experimental situation.

The essence of the technique proposed is the measurement of force acting on a plate moving in a gas. The plate motion can be ensured by free oscillations. In the present work, we measured the damping coefficient of free linear oscillations of an elastic plate in the free-molecular regime with varied gas pressure. The measurement path of the experimental setup is schematically shown in Fig. 3.1. The sensor is fabricated from a plate of microcontoured single-crystal silicon by the MEMS technology. This allowed an almost perfect attachment of the elastic part of the plate 5 × 5 mm and obtaining rather stable damping coefficients of plate oscillations $\beta = (0.020 \pm 0.002)$ sec^{-1} under conditions of ultrahigh vacuum (of the order of 10^{-7} Pa). The thicker part of the plate, which does not directly participate in the momentum-transfer process, is fixed by assembling screws used in ultrahigh vacuum engineering. The elastic plate together

with the fixed electrode forms an electric capacitor of about 15 pF, which is connected to the oscillating LC generator with a resonance frequency of about 10 MHz. The initial oscillations of the elastic plate are excited by the electric field between the sensor and fixed electrode by means of a specially designed system of self-induced oscillations. The excitation system serves as a chain of feedback and a source of external energy. The natural oscillation frequency of the elastic plate is about 1250 Hz.
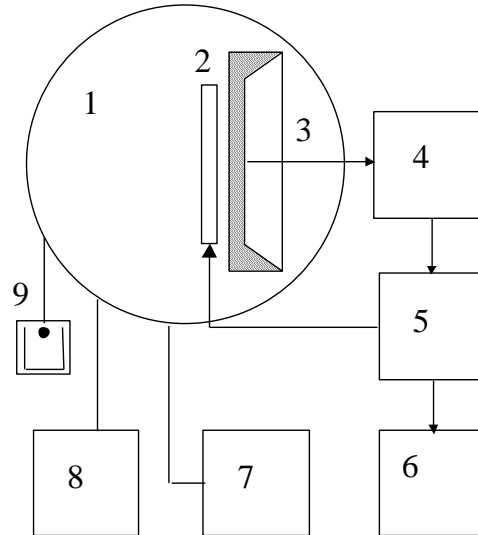

Fig. 3.1. Measurement path of the experimental setup: 1) fixed electrode; 2) microcontoured silicon plate; 3) high-frequency LC generator; 4) frequency detector; 5) selective amplifier; 6) oscillation-generation system; 7) analog-to-digital converter; 8) computer.
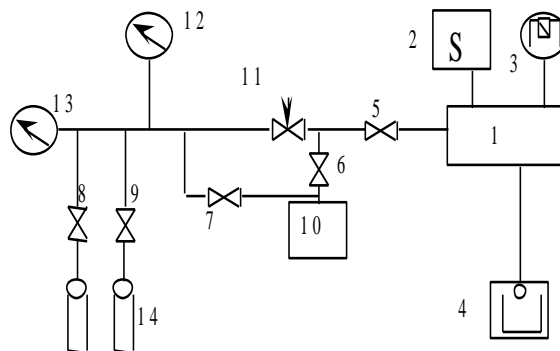

Fig. 3.2. Vacuum chamber and gas-inlet system: 1) vacuum chamber; 2) monopole mass spectrometer; 3) vacuum pressure gauge; 4) sputter-ion pump; 5–9) vacuum valves; 10) backing pump system; 11) gas-inlet valve; 12) optical membrane gauge; 13) thermocouple vacuum gauge; 14) gas reservoirs.

The microcontoured silicon plate and the fixed electrode are mounted vertically in the vacuum chamber, which is shown in Fig. 3.2 together with the gas-inlet system. The gas is evacuated from the vacuum chamber by a sputter-ion pump with a pumping velocity of 100 liters/sec. The residual pressure in the vacuum chamber is measured by a Penning vacuum gauge and reaches less than 10^{-7} Pa. The gas composition is controlled by a monopole mass spectrometer for pressures lower than 10^{-3} Pa. The vacuum chamber is connected to the gas-inlet system through a valve. Preliminary evacuation is performed by the backing pump system consisting of two adsorption pumps and a mechanical vacuum pump. The gas pressure in the inlet system is measured by an optical membrane gauge and a thermocouple vacuum gauge.

Measurement of the damping coefficient of free linear oscillations of the elastic plate with varied gas pressure reduces to registration of the value of a capacitor formed by the elastic plate and the fixed electrode and included into the oscillating circuit of the LC generator.

For NMAC determination, the measurements are performed with fixed values of gas pressure. Except for the standard procedure of cleansing after the final stage of fabrication, the sensor surface received no other treatment.

The prior measurements based on the use of this experimental approach have demonstrated significant change in damping process. In particular, the frequency shift for wide range of Knudsen numbers has been observed that confirms high sensitivity of this method to gas/surface interaction parameters (Figs.2.3, 2.4).
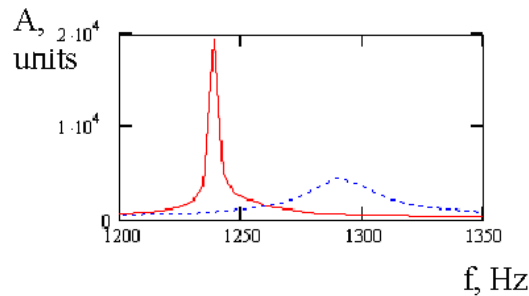

Fig.3.3. Frequency shift as a result of gas pressure change (hard line – 1Pa, dotted line – 10Pa).
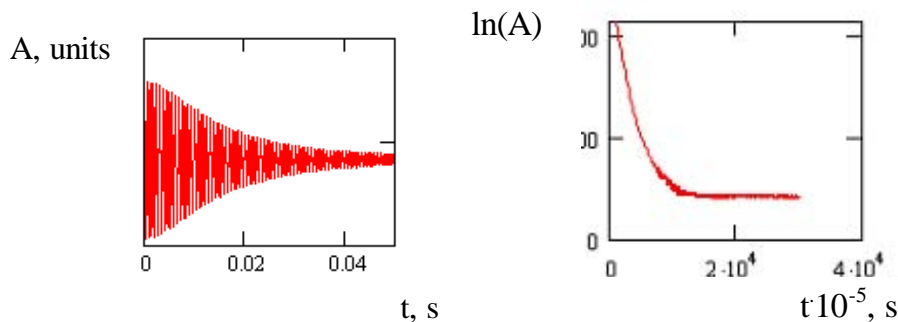

Fig.3.4. Decay curve and its logarithms at 10 Pa.

To take into account adsorption influence the basic QCM principles are used. According to Sauerbrey's assumptions regarding the mass/frequency shift relation the density of deposited thin layer and elastic modulus are such that it can be treated approximately as an extension of the silicon crystal. The mass of the adsorbed molecules Δm would be equivalent to an increase in the mass m of the elastic plate. Thus the resonator thickness h is connected with its mass as

$$h = \frac{m}{F\rho},$$
(3.a)

where F is an elastic plate square, ρ is a density of the silicon single crystal plate. The resonant frequency of unloaded square plate can be presented as

$$F = K \cdot h,$$
(3.2)

where K is the constant depending on the Poisson's ratio, the Young's modulus, the elastic plate square size, the density of the silicon single crystal.

Thus a frequency change Δf can be connected with a thickness change Δh by the following correlation

$$\frac{\Delta f}{f} = \frac{\Delta h}{h} .$$
(3.3)

Taking into account the earlier obtained expression for the normal momentum accommodation coefficient α_n the decay time constant β can be presented finally as

$$\beta = \frac{(2 - \alpha_n)}{\rho h \left(1 + \frac{\Delta f}{f}\right)} P \sqrt{\frac{2m_g}{\pi k T}} ,$$
(3.4)

where P is a gas pressure, m_g is a gas molecule mass, k is the Boltzmann constant, T is a temperature.

The preliminary measurements of time frequency dependence and damping process of free elastic plate vibrations have carried out at ultrahigh vacuum conditions. The temperature dependence of frequency and spectrum of vibrations are presented in Fig.3.5. The spectrum is obtained as a result of the Fast Fourier Transform (FFT) application to signal processing at the rate of 10^4 samples per second.

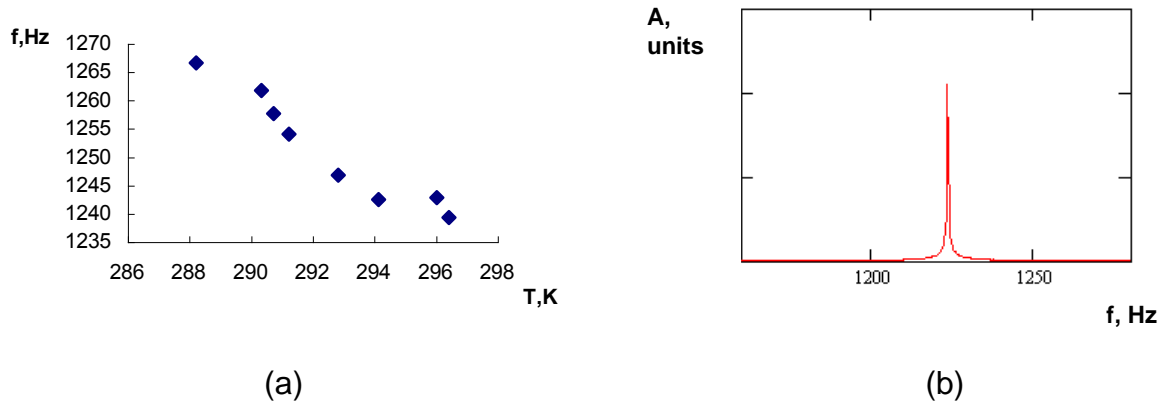(a)   (b)

Fig. 3.5. The temperature dependence of natural frequency (a) and frequency spectrum (b) of the elastic plate vibrations: A is amplitude of the signal in relative units.

The absence of high mode in frequency spectrum gives an opportunity to be limited by the linear vibrations of the elastic plate only.

By the use of SLM the following value of the decay time coefficient at ultrahigh vacuum conditions has been obtained

$$\beta = (0.020 \pm 0.002) \sec^{-1} .$$

The measurement of the gas pressure in the vacuum chamber is an important step of the measuring technique. Unfortunately, construction features of the elastic silicon single-crystal plate do not permit to realize the measurements in the pressure range upper than 10^{-2} Pa. The reason is connected with a small damping time that leads to difficulties in the decay time coefficient determination.

The change in residual gas pressure at switched off means of gas evacuation provides natural opportunity to carry out experiment and to get gas pressure dependence of measuring parameters.

During the total time of experiment of more than three months the gas composition of the chamber atmosphere was not changed significantly and is consisted of 96% N_2.

At the gas pressure of about 0.1 Pa the measurements was carried out with the rate of 1/15 musec-1 and were processed by FFT. Frequency spectrum of plate vibrations excited by electrostatic field and one at damping conditions are presented in Fig.3.6. In this case the decay time coefficient gets the value of $\beta = (8.6 \pm 0.7)\sec^{-1}$.

(a)   (b)
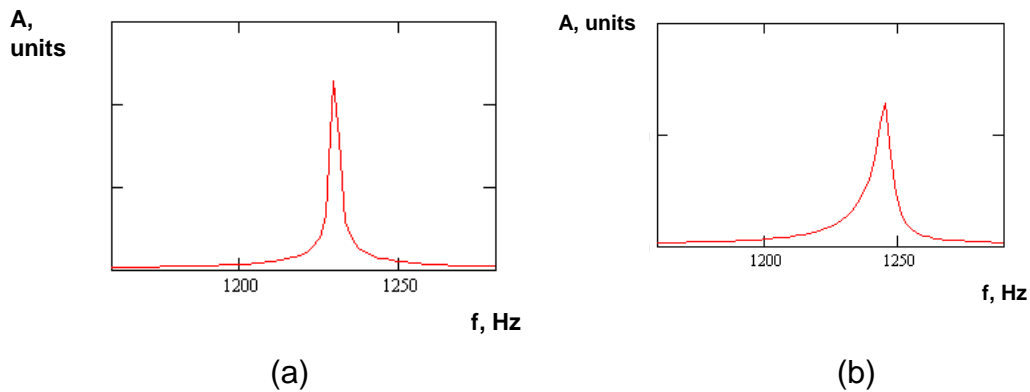
FIG. 3.6. Frequency spectrum of plate vibrations excited by electrostatic field (a) and one at damping conditions (b). This is the Style for Figure Captions. Center this text if it doesn't run for more than one line.

The analysis of the results gives the frequency shift of about 17 Hz that is corresponds to 1,4%. The frequency increase agrees with theoretical predictions. The quantitative estimation is not available at this stage because of the problem of absolute gas pressure measurements.

The obtained results approve the initial assumptions and demonstrate agreement between theory and experiment. The direction of frequency shift coincides with the theory prediction.

The quantitative estimation problem can be solved by geometric parameters optimization technique.

The problem of reception of quantitative estimations can be solved by change of the geometrical sizes of an elastic plate. This decision is closely connected to fabricating technique of Silicon single-crystal elastic plate. MEMS technology achievements can be useful and fruitful.
The other way of decision of the problem is connected with pressure data acquisition. Particularly it can be achieved by application of new device such as a dynamic technique.

Due to relative simplicity combined with high efficiency variation methods are widely used for studying an elastic body deformation. In order to write down the equation describing process of the plate movement in a gas it is convenient to construct functional of the moving plate and determine its extreme by the use of variation Ritz method.

Functional variation equation written for whole volume of the elastic body has the following form

$$\delta \int_{t_0}^{t} \int_{v} (\rho \frac{\upsilon^2}{2} + U(\vec{X})) dv dt + \delta B = 0 , \qquad (3.5)$$

$$\delta B = \int_{\Omega} (\vec{p}^n)^i \, \delta w_i d\sigma + \int_{v} \rho F_i \delta w_i dv - \int_{v} \rho s \delta T dv , \qquad (3.6)$$

where $U(\vec{X})$ -potential energy of volume element of the body, ρ -material density, t_0 , t - initial and present time respectively, $\vec{\upsilon}$ -velocity of the volume element, $\delta w_i(\vec{X})$ - displacement deviations, dv -volume element, δT -temperature deviations of elasticity body, $\vec{F}$ -mass force applied to the body, s -entropy of volume element, $\vec{X} = (x_1, x_2, x_3)$, Ω - surface area,

$$(\vec{p}^n)^i = p_{ij} \vec{n}_j ,$$

here $\vec{n}_j$ - normal vector of j axis, p_{ij} - stress tensor.

Taking into account that body temperature is constant last item in expression for δB can be discarded. Some principal components of p_{ij} and $U(\vec{X})$ must be determined.

In this study the free damping oscillations of the square thin plate with rigidly fixed edges are considered. The plate is placed in the rarefied gas. Free molecular gas conditions are provided by high ratio of mean free path of gas molecules to linear plate dimensions.

Accepting small curvature of the plate for the first degree of approximation one can neglect tangential stress to the plate surface.

According to the assumption regarding smallness of the plate curvature the normal vector to any element of the surface can be considered as parallel to z-axis (Figure 3.7). Inside the moving plate there is so-called "neutral layer", where any tensions and compressions are absent. The neutral layer point's movement is described by transverse displacement of the in-plate co-ordinates x and y as $\vec{\omega}$.
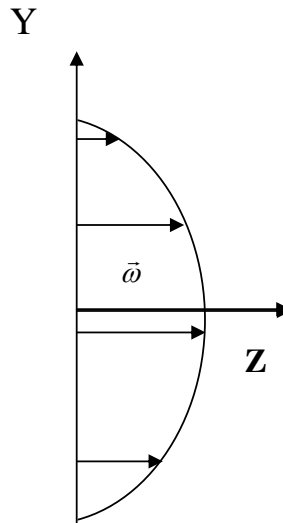

FIG. 3.7. Profile the neutral layer point's displacements of the plate.

Therefore, the vector of displacements of points of the neutral layer can be presented as

$$\bar{\omega} = (0,0,\omega_0) \,,$$

where $\omega_0 = f(x,y,t)$. For small displacement the points of the neutral layer move in perpendicular directions relatively to the plane of initial plate position.

Let us introduce the coordinate system x', y', z' connected with the moving plate surface.

If to take into account that unit normal to any surface element is parallel to z-axes the components of molecule velocities can be written as

$$\begin{cases} \vartheta_x = \vartheta_{x'} \\ \vartheta_y = \vartheta_{y'} \\ \vartheta_z = \vartheta_{z'} \pm \dfrac{\partial \omega_0}{\partial t} \end{cases} \tag{3.7}$$

The different sign at $\dfrac{\partial \omega_0}{\partial t}$ connected with the opposite plate sides.

The normal momentum flux to the elementary surface area can be expressed as

$$p_i = \frac{\rho_\infty R T_\infty}{\pi^{1/2}} (B\exp(-B^2) + \pi^{1/2}(\frac{1}{2} + B^2)(1 + erf(B)) \,, \tag{3.8}$$

where $\beta = \dfrac{1}{\sqrt{2RT_\infty}}$; $B = \pm\dfrac{1}{\sqrt{2RT_\infty}}\dfrac{\partial \omega_0}{\partial t}$, ρ_∞ and T_∞ - density and temperature of undisturbed gas correspondingly, R - gas constant.

According to accepted Knudsen definition of accommodation coefficient the equation for normal momentum flux created by reflected molecules can be presented as

$$p_r = (1-\alpha_n)p_i + \alpha_n p_w \,. \tag{3.9}$$

The expression for total normal momentum flux applied to the plate has a view as

$$p = p_i + p_r = (2-\alpha_n)p_i + \alpha_n p_w \tag{3.10}$$

where α_n - so-called normal momentum accommodation coefficient, p_i - normal momentum flux created by incident molecules, p_w - normal momentum flux caused by the influence of reflected molecule having Maxwell distribution function with zero macroscopic velocity and with the temperature of the surface.

Assuming velocity loss of diffuse reflected molecules that leave the surface with equilibrium distribution function one could write p_w as

$$p_w = \frac{m}{2}\sqrt{2\pi R T_\infty} N_i \,, \tag{3.11}$$

where m - molecule mass, N_i - number of molecules striking the unit surface per unit time:

$$N_i = n_\infty \sqrt{\frac{RT_\infty}{2\pi}} (\exp(-B^2) + \sqrt{\pi} B(1 + erf(B))), \tag{3.12}$$

where n_∞ - gas numerical density at infinity.

Oscillations are believed to be at quasi-steady condition. Hence, it can be considered that $B^2 \ll 1$.

Finally, the normal pressure to the surface unit becomes

$$P = P_\infty \pm \rho_\infty \sqrt{\frac{2RT_\infty}{\pi}} \frac{\partial \omega_0}{\partial t} (\alpha_n \frac{\pi}{4} + 2 - \alpha_n), \tag{3.13}$$

P_∞ - gas pressure at infinity, $\rho_\infty = n_\infty m$.

Elastic body presents the plate of cubic syngony with (100) orientation.

Density of strain energy U in Hookian approximation is a quadratic function of components of the deformation tensor:

$$U = \frac{1}{2} \sum_{\lambda=1}^{6} \sum_{\mu=1}^{6} C_{\lambda\mu} e_\lambda e_\mu, \tag{3.14}$$

where e_λ, e_μ - deformation tensors, λ, μ indexes are determined as
$$1 = xx,\ 2 = yy,\ 3 = zz,\ 4 = yz,\ 5 = zx,\ 6 = xy,$$

$C_{\lambda\mu}$ - components of the elasticity tensor (cubic syngony) can be written in a matrix form:

$$C_{\lambda\mu} = \begin{pmatrix} c_{11} & c_{12} & c_{12} & 0 & 0 & 0 \\ c_{12} & c_{11} & c_{12} & 0 & 0 & 0 \\ c_{12} & c_{12} & c_{11} & 0 & 0 & 0 \\ 0 & 0 & 0 & c_{44} & 0 & 0 \\ 0 & 0 & 0 & 0 & c_{44} & 0 \\ 0 & 0 & 0 & 0 & 0 & c_{44} \end{pmatrix}.$$

Hence,

$$U = \frac{1}{2} c_{11}(e_{xx}^2 + e_{yy}^2 + e_{zz}^2) + \frac{1}{2} c_{44}(e_{yz}^2 + e_{zx}^2 + e_{xy}^2) + c_{12}(e_{yy}e_{zz} + e_{zz}e_{xx} + e_{xx}e_{yy}). \tag{3.15}$$

Taking into account assumptions made above and using correspondent expressions one can obtain

$$e_{xx} = -z \frac{\partial^2 \omega_0}{\partial x^2};\ e_{yy} = -z \frac{\partial^2 \omega_0}{\partial y^2};\ e_{xy} = -2z \frac{\partial^2 \omega_0}{\partial x \partial y};\ e_{zz} = e_{xz} = e_{yz} = 0. \tag{3.16}$$

Expression for U can be obtained by replacing (3.16) in (3.15)

$$U = \frac{1}{2} c_{11} z^2 ((\frac{\partial^2 \omega_0}{\partial x^2})^2 + (\frac{\partial^2 \omega_0}{\partial y^2})^2) + 2c_{44} z^2 (\frac{\partial^2 \omega_0}{\partial x \partial y})^2 + c_{12} z^2 \frac{\partial^2 \omega_0}{\partial x^2} \frac{\partial^2 \omega_0}{\partial y^2}. \tag{3.17}$$

Finally for the whole plate it becomes:

$$U = \frac{h^3}{3} \iint \left(\frac{1}{2} c_{11} \left(\left(\frac{\partial^2 \omega_0}{\partial x^2} \right)^2 + \left(\frac{\partial^2 \omega_0}{\partial y^2} \right)^2 \right) + 2 c_{44} \left(\frac{\partial^2 \omega_0}{\partial x \partial y} \right)^2 + c_{12} \frac{\partial^2 \omega_0}{\partial x^2} \frac{\partial^2 \omega_0}{\partial y^2} \right) dx dy .$$ (3.18)

Present consideration of the variation task is based on following assumptions.
   a) The damping of the plate oscillations caused by internal stresses is negligible in comparison with the damping due to external forces due to gas-surface interactions.
   b) The plate produces the small oscillations in strongly perpendicular directions to the plane of unmoved plate.
   c) The oscillations are believed to have a single harmonic.

Equations (2.5) and (2.6) are transformed to the following form:

$$\delta \int_{t_0}^{t_1} (T+U)dt + 2\int_{t_0}^{t_1} \iint_{\Omega} \rho_\infty \sqrt{\frac{2RT}{\pi}} \frac{\partial \omega_0}{\partial t} (\alpha_n \frac{\pi}{4} + 2 - \alpha_n) \delta \omega_0 dx dy dt = 0 ,$$ (3.19)

where T -kinetic energy of the plate determined as

$$T = \frac{\rho h}{2} \iint_{\Omega} (\frac{\partial \omega_0}{\partial t})^2 dx dy ,$$ (3.20)

here h - plate thickness.

Determination of the extreme of the functional (2.19) is made by the Ritz method.

The minimization form is taken in the following view:

$$\omega_0(x, y, t) = \sum_{n,m} a_{nm}(t) \sin^2 \frac{\pi x n}{a} \sin^2 \frac{\pi y m}{a} ,$$ (3.21)

where a - side length of the plate, n , $m \in (0, \infty)$.

This form must satisfy to boundary conditions corresponding to the case of the plate with rigidly fixed edges.

$$\omega_0 = 0 \text{ at } x = 0, x = a \text{ and } y = 0, y = a ;$$

$$\frac{\partial \omega_0}{\partial x} = 0 \text{ at } x = 0, x = a ; \quad \frac{\partial \omega_0}{\partial y} = 0 \text{ at } y = 0, y = a .$$

In addition to the conditions mentioned above, function $\omega_0(x, y, t)$ in continuous region $G \in [0, a] \times [0, a]$ at $n = 1, m = 1$ has a single extreme point in the center of the plate $(\frac{a}{2}; \frac{a}{2})$, which corresponds to the oscillation condition with single harmonic and the basis functions $\sin^2 \frac{\pi x n}{a}$ and $\sin^2 \frac{\pi y m}{a}$ have the spanning property.

Using correspondent replacements and some lemmas of variation calculus, one can obtain the definitive equation

$$\rho h a^2 \frac{d^2 a(t)}{dt^2} + 2\rho_\infty \sqrt{\frac{2RT}{\pi}} (\alpha_n \frac{\pi}{4} + 2 - \alpha_n) a^2 \frac{da(t)}{dt} + \frac{32 h^3 \pi^4}{27 a^2} (3c_{11} + 2c_{22} + c_{12}) a(t) = 0 .$$ (3.22)

Finally, the damping coefficient of plate oscillations can be presented as a function of normal momentum accommodation coefficient by the following way

$$\beta = \frac{\rho_{\infty}}{\rho h} \sqrt{\frac{2RT}{\pi}} (\alpha_n \frac{\pi}{4} + 2 - \alpha_n). \qquad (3.23)$$

This expression can be compared with the result obtained earlier:

$$\beta = \frac{\rho_{\infty}}{\rho h} \sqrt{\frac{2RT}{\pi}} (2 - \alpha_n). \qquad (3.24)$$

The normal momentum accommodation coefficient dependence of β in relative units obtained from equations (3.23) and (3.24) is shown in Figure 3.8.
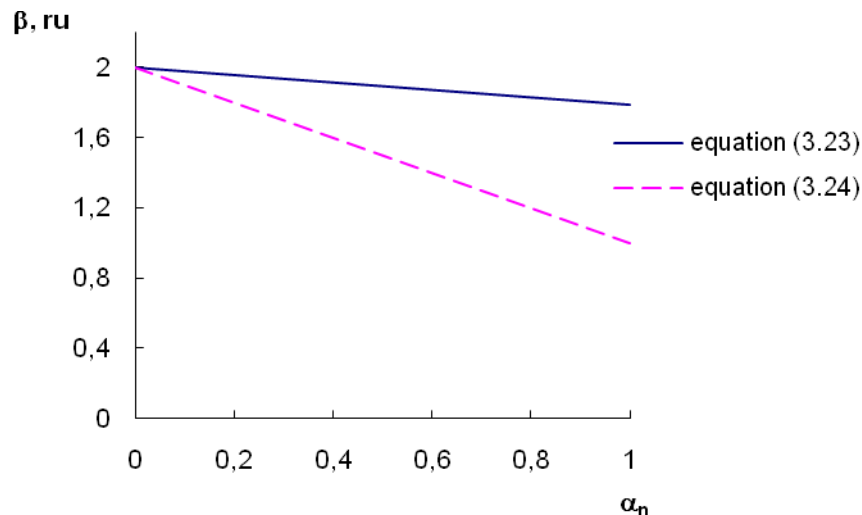

Fig. 3.8. Normal momentum accommodation coefficient dependence of β related to $\rho_{\infty}\sqrt{\frac{2RT}{\pi}} \Big/ \rho h$ for equations (3.23) and (3.24).

The contribution of normal momentum accommodation in damping coefficient according to equation (3.23) is about 20% at $\alpha_n \approx 1$. The difference between β obtained from equations (3.23) and (3.24) can reach up to 78%.

Thus, equation (3.23) is more preferable to processing experimental data especially for the gases with normal momentum accommodation coefficient close to one.

YEAR 2:

TASK 4: ENERGY ACCOMMODATION MEASUREMENTS.

Figures 4.1a and 4.2b show the measured power supplied to the tungsten sample in Argon and CO_2, respectively. Each symbol represents the average of more than 100 data points acquired by the computer controlled heating and temperature stabilization system operating at an input sampling rate of 50 kHz.
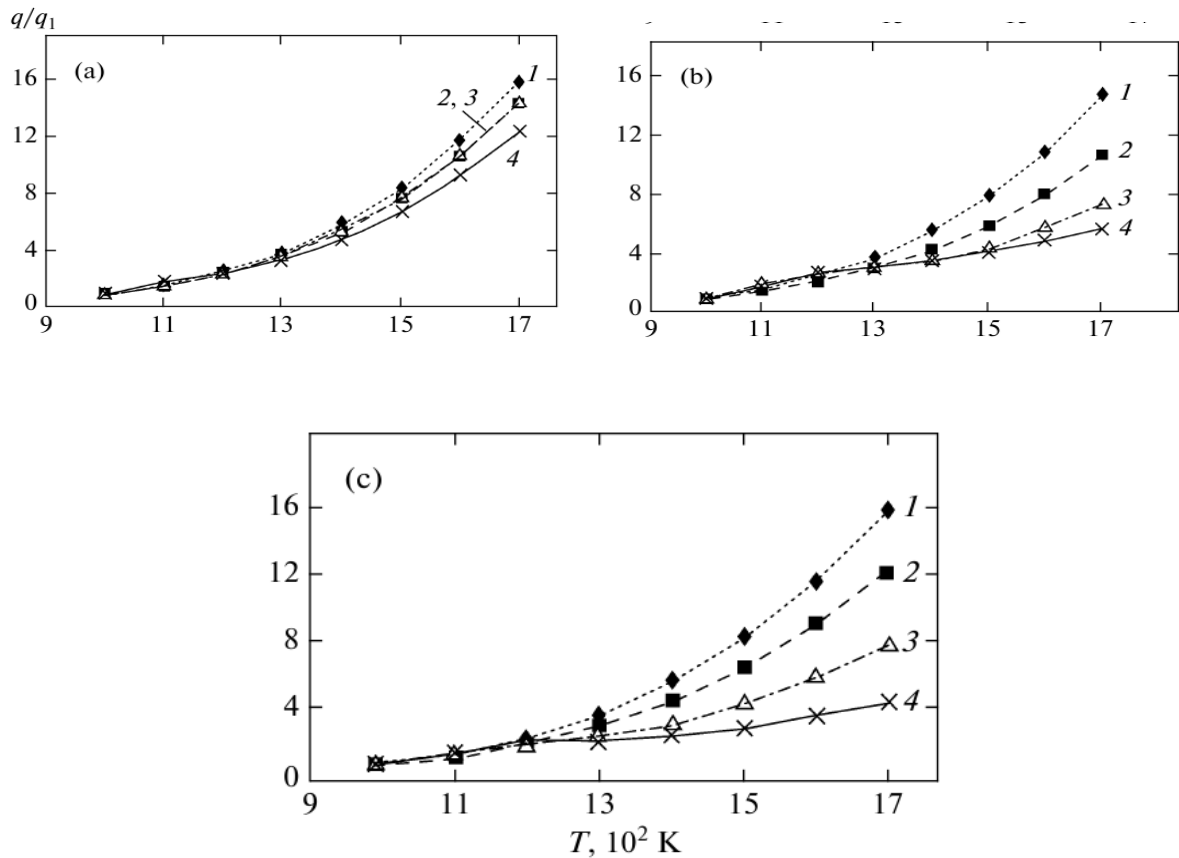
Fig. 4.1. Electric power supplied to sample vs. temperature
for (a) argon, (b) CO2, and (c) at discharge current J =
(1) 0, (2) 40, (3) 100, and (4) 200 mA.

To facilitate analysis, the data are represented as the ratios q/q_1 between the powers measured at particular temperature and T = 1000 K. The curves obtained for different gases exhibit different behavior, particularly at high temperatures.

The measurement parameter settings are such that the relative error does not exceed 5%.

The power supplied to the glow discharge also has an absolute error due to the filament sputtering during the measurements performed at operating values of current and voltage. This is supported by the results of preliminary scanning electron microscopy studies. Additional indirect evidence is provided by the fact that the sample resistance increases by approximately 10% over a measurement cycle, which corresponds to a decrease in wire radius by up to 3%.

We have also performed experiments on glow discharge in air (see Fig.4.1c). Their results, being similar to those obtained for CO_2 plasma, suggest that the characteristics of heat transfer at high temperatures strongly depend on the composition of the molecular gas plasma produced in the glow discharge. The analysis that follows focuses on heat transfer in Argon and CO_2 plasmas.

The most important plasma processes contributing to heat transfer across the tungsten surface include radiation, sputtering, molecular heat conduction, and heterogeneous recombination.

The radiative heat fluxes are approximately equal for both gases. Indeed, even if a layer of some compound forms on the filament surface in CO_2 atmosphere, the ensuing change in emissivity can be neglected in view of the concurrent sputtering; i.e., the radiative heat flux can be assumed to depend only on the filament temperature.

Neither physical sputtering, nor chemical sputtering, nor sublimation can be singled out as a dominant process responsible for material loss when comparing the two gases under study. Furthermore, the sputtering rate constant is independent of sample temperature far from the sublimation point, and sputtering has similar characteristics in argon and CO_2 atmospheres when all other parameters are equal.

Since the Knudsen number for the actual geometry used in our experiments is Kn > 10, analysis can be restricted to free molecular heat transfer. The gases under study have similar molecular masses, and preliminary estimates give a degree of ionization varying between 10^{-5} and 10^{-3}. Therefore, the thermal accommodation coefficients for Ar–W and CO_2–W systems are approximately equal according to Baule's theory.

Based on the discussion above, we suggest that the experimentally found difference in heat transfer between the gases can be attributed to heterogeneous recombination processes, which are significant at a temperature of 1700 K.

Consider the normalized supplied power q/q1 plotted as a function of discharge current for CO_2 and Argon in Fig.4.2. The slopes of the lines, obtained by least squares interpolation, differ by a factor of more than 2.
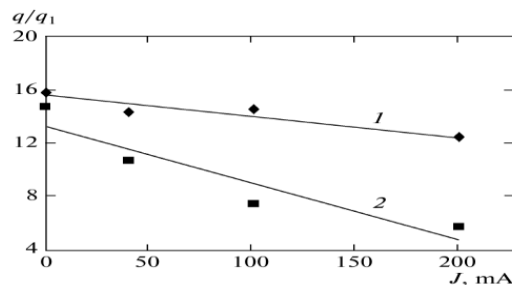

Fig. 4.2. Electric power supplied to tungsten wire vs. discharge current at sample temperature T = 1700 K: (1) argon; (2) CO_2.

In the case of argon, the linear interpolation slopeis determined by the heating of the discharge chamber walls throughout the measurement process, which can be caused both by radiation from the tungsten wire and by heat transfer from the plasma. These effects can be taken into account by introducing certain changes into the measurement procedure.

Glow discharge in carbon dioxide is characterized by complex plasma composition strongly depending on discharge current. The dominant mechanism of dissociation is the following:

$$CO_2 + e \longrightarrow CO_2^- \longrightarrow CO + O^-.$$
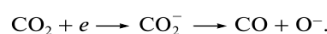
Its products can obviously play an important role in plasma–surface interaction.

Heterogeneous recombination, which significantly contributes to the heat transfer between the tungsten filament and the CO2 plasma, may follow two mechanisms: the Eley–Rideal mechanism (reaction between a gas phase species and an adsorbed one) and the Langmuir–Hinshelwood mechanism (reaction between adsorbed molecules).

A general analysis may include a wide variety of recombination–dissociation and exchange reactions. However, the available experimental data are not sufficient to single out a dominant mechanism.

Our experimental results demonstrate that the hot filament method can be used under glow discharge conditions to examine characteristics of heat transfer between low temperature monatomic or molecular gas plasma and a solid surface.

A qualitative analysis of the measured results suggests that heterogeneous recombination plays a significant role in plasmas of CO2 and other polyatomic gases, such as those contained in air.

Task 5: Surface structure effects on gas flow rate in channels.

One of the factors that have a great influence on gas/surface interaction and as a result on heat and mass exchange in a gas/surface system is surface roughness. This effect has been studied experimentally earlier and described with the use of different surface structure models later. The main problem of surface structure modeling at least at the first steps was a lack of the information on features of real surfaces. Significant progress in experimental technique, in a particular, numerous realizations of Scanning Probe Microscopy open new opportunities in surface diagnostics at micro- and nano- scales. Because of essential increase in a role that gas/surface interaction plays at miniaturization of gas dynamics systems the problem becomes rather topical.

In this study an attempt to describe gas particles scattering by the real Si-based surface has been made with the use of DSCM approach. The surface morphology of the sample has been studied by Atomic Force Microscopy (AFM) that provides obtaining such characteristics of the surface as mean square height of micro roughness, fractal dimension and micro roughness distribution function. The surface of the sample studied by AFM presents area of 20x20 mkm and characterizes by 160 thousand points. The surface has been simulated by triangulations which are necessary to calculate coordinates of crossing points of particle trajectories with a surface. Fragment of the surface simulated according to AFM data is presented in Fig.5.1.

DSMC in a probe particle version has been realized for modeling of gas scattering by a surface at various parameters of micro roughness considering diffuse or specula reflection of gas particles from a separate elementary plate of a rough surface. As a first step monochromatic gas particles flow directed to the surface at various angles is considered. The next step supposes to consider gas flow in a channel and take into account real distribution function of micro roughness and gas molecule velocity distribution function on an input in the channel as well.

As a result of the study index ellipsoids (scattering indicatrix) for various angles of incident particles and parameters of surface roughness have been obtained. Lobular and completely diffuse scattering presented in Fig.5.2 demonstrate effect of variation in surface roughness factors. Test calculations confirm well known fact of completely diffuse scattering of monochromatic particles flow with thermal energy by a rough

surface and specula reflection in the case of a smooth surface. It has been found that number of "particle – separate rough surface side" collisions depends on surface roughness parameters and as a result influences on scattering indicatrix. Fig.5.3 illustrates velocity distribution function for reflected particles simulated on the basis of 100 thousand tests.
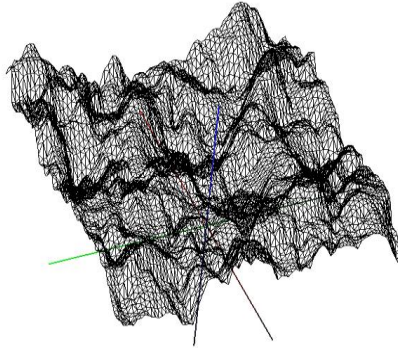

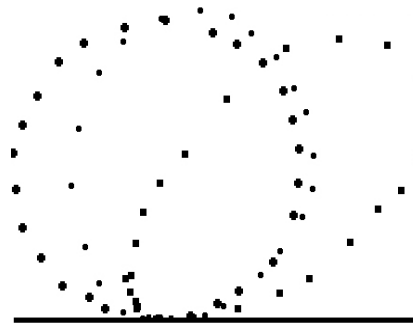| Fig.5.1. Surface structure simulated by triangulations according to AFM data | Fig.5.2. Scattering indicatrix as a function of average relative height of surface roughness: ■, ·, ● – 1, 2, and > 3, respectively | Fig.5.3. Gas velocity distribution function for reflected particles (y-component in relation to most probable value) |

One of questions of principle which was put at this stage consisted in finding out how much gas flow rate is sensitive to character of surface structure at the same size of average height of microroughness. The thing is in some cases the channels have specially prepared surface with regular structure. In other cases we have real surfaces with statistical distribution of microroughness.
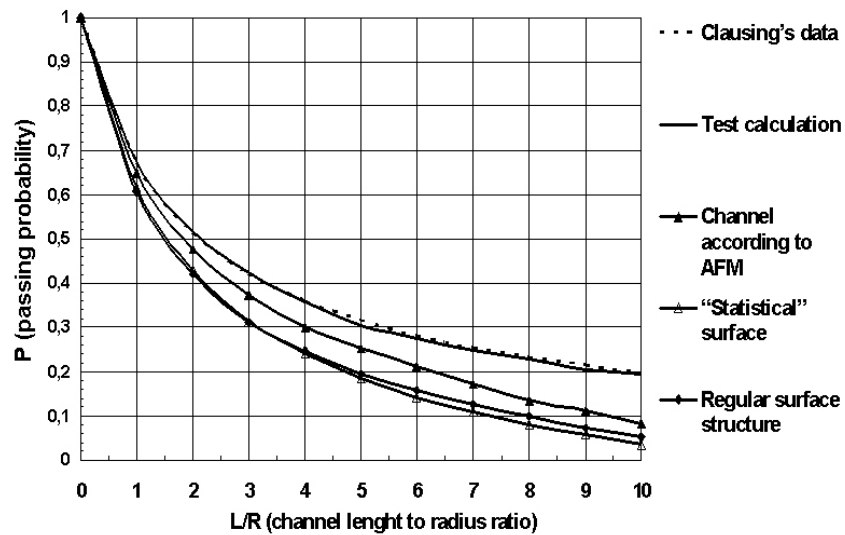
Fig.5.4. Calculated results for passing probability of cylindrical channels with various surface structures.

As it follows from Fig.5.4 there is an essential distinction between the results obtained for smooth surface (Clausing's data) and for surfaces with regular or statistical structure as well as for surface reconstructed according to AFM data. It means that the use of simplified model of a surface as it realized in many cases can bring considerable errors in calculation of gas flow rate.

Task 6: Surface chemical composition effects on molecular heat transfer.

The experimental setup created for realization of this stage provided measurements with ultrahigh vacuum conditions up to 10^{-10} mmHg as well as with means of surface and gas phase diagnostics by the use of vacuum system based on the helium cryogen pump, mass-spectrometer and Auger-electron spectrometer built in measuring chamber.

The situation observed in measuring system during surface purification process and thermal accommodation measurements in *He-W* system is presented in Figs.6.1-6.3.
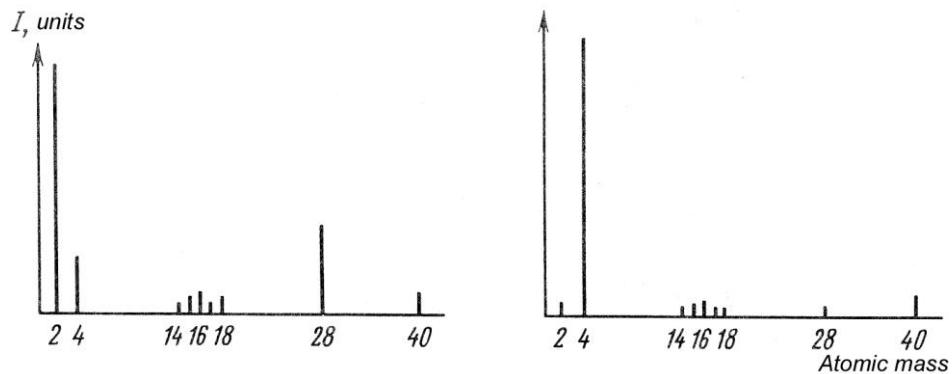

Fig. 6.1. Mass spectrum in vacuum system before (left) and after (right) leak-in *He*.
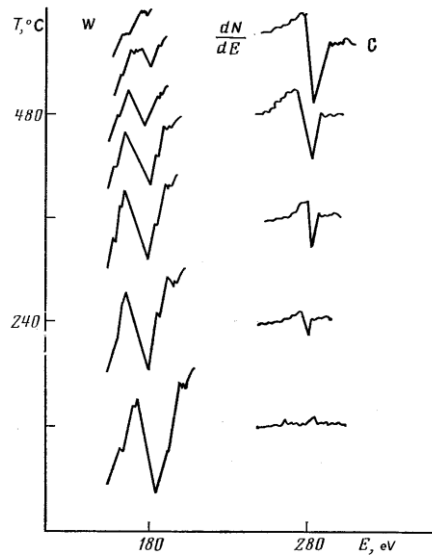
Fig.6.2. Energy peaks of Auger-electrons at the process of tungsten surface covering by hydrocarbons: bottom peaks – "clean" surface; top peaks – "dirty" surface.
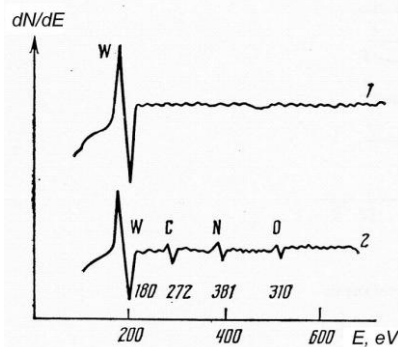

Fig.6.3. Auger spectrum for *W* wire sample at different stages of cleaning: *1* - surface after series of purification cycles; *2* – partially contaminated surface with *C, N, O* atom complexes.

The intensity of the peaks in Fig.6.2 and Fig.6.3 corresponds to number of Auger-electrons that reflects concentration of atoms on the surface. The term "dirty" surface means here the surface at initial conditions before applying special purification measures.

The value of thermal accommodation coefficient α_E at the process of surface contamination removal changes from ~ 0.45 for the surface without special treatment (typical value for "dirty" surfaces) to ~0.02. Purification cycles included annealing at ultrahigh vacuum conditions and chemical reduction in hydrogen environment. Dependence of αE on surface temperature and surface coverage θ (surface fraction covered by adsorbed gases) for *He-W* system is presented in Fig.6.4.
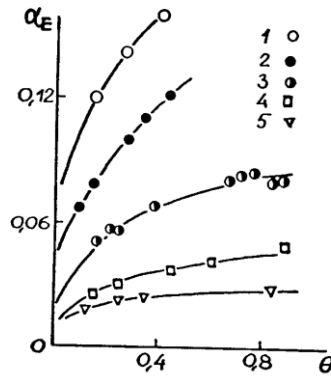
Fig.6.4. Thermal accommodation coefficient α_E as a function of θ and surface temperature:
1 – 298 K; 2 – 446 K; 3 – 968 K; 4 – 1650 K; 5 – 2020 K.

On the basis of classical knowledge about movement of atoms and lattice theory of F. Goodman and G. Wachman the program modeling equilibrium and nonequilibrium scattering of helium atoms on a three-dimensional crystal tungsten lattice taking into account partial surface coverage with adsorbed oxygen atoms is developed. The modeling scheme is presented in Fig.6.5.
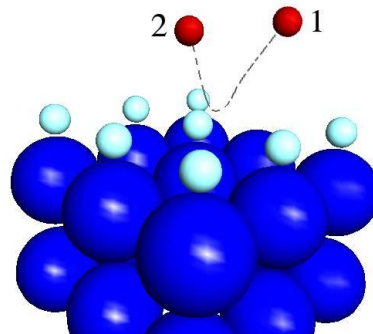

Fig.6.5. Scattering of *He* atom on *W* lattice partially covered by oxygen atoms due to adsorption, $\theta \sim 0.8$: *1, 2* - positions of *He* atom (initial and finite, respectively).

The scattering model is constructed on the basis of following assumptions: a) atoms of gas and a solid body represent spheres, their radius and mass correspond to characteristics of real atoms; b) W sample is modeled as crystal with bcc lattice structure producing thermal vibrations at temperature Ts; c) forces of interaction between atoms of a crystal are modeled only as ones between the nearest neighbors; d) particles of gas falling on a surface represent the Maxwell's flow at temperature Tg; e) interaction force between atom He and a solid body is calculated taking into account all atoms of a crystal and the atoms adsorbed on it; f) adsorbate is modeled by atoms of oxygen as their primary presence on a surface proves to be true by the data of the electron-spectroscopic analysis; g) the case of thermal scattering of atoms on a crystal surface with $E_i < 0.1$ eV is considered as far as scattering of particles with higher energy demands quantum-mechanical interpretation; h) influence of every possible directions of crystal axes on scattering process is not considered, otherwise, atom of gas interacts with a flat surface. Thus, the data obtained during modeling represents integrated behavior of gas – surface system that is realized during all possible processes of scattering.

Interaction of helium atom with a solid body is described by potential function of pair interaction between gas atom and each atom of a solid body (including the adsorbed atoms). As interaction potential between atoms of all types the Morze potential has been chosen.

In terms of energy accommodation coefficient αE an efficiency of molecular heat exchange of helium with clean and partially covered by adsorbed oxygen atoms tungsten surface is calculated for various temperatures. The calculated temperature dependences are compared with the data obtained in experiments with surface diagnostics. Within the limits of the developed approach the results of calculations are in a satisfactory agreement with experimental data obtained for equilibrium αE and clean surface (Fig.6.6.) as well as for nonequilibrium αE and a surface partially covered by oxygen atoms (Fig.6.7).
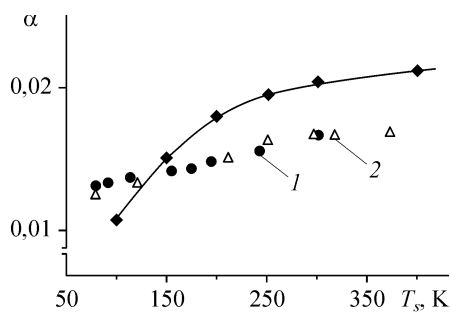

Fig.6.6. "Equilibrium" α_E for clean surface. Simulation (bold line) and experiment:
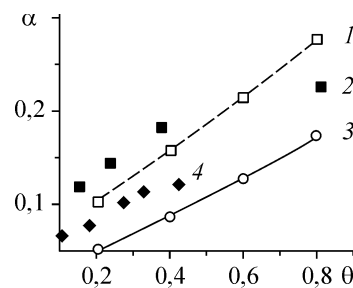*1* - L.B. Thomas, 1967
2 - J. Kouptsidis et al, 1970.

Fig.6.7. "Nonequillibrium" α_E for contaminated surface $T_g= 300K$:
Ts=298K; *1*- simulation,
2- experiment,
Ts=446K; *3*- simulation,
4- experiment.

Task 7: Surface chemical composition effects on freemolecular gas flow in channel.

In our case the surface preparation procedure is based on evaporation and deposition of metal on internal surface of a cylindrical channel. As the investigated channel the Pyrex glass cylindrical channel in diameter of 6.4 mm and length 150 mm has been taken. Titanium filament with 0.6 mm in diameter is stretched along its axis. Heating of the wire is reached by the use of electric current. The change in chemical composition of the surface is controlled by Auger-electron spectroscopy using special pilot sample (witness) that is situated near the channel and simultaneously exposed. To arrange the guaranteed surface coverage with adsorbate a special oxygen source has been used.

The results of surface analysis for two situations ("dirty" and "clean" surface) are presented in Fig.7.1. Similar spectrum in vacuum system one can observe practically in all cases when special measures for purification are not applied. This result is expected if take into account mass-spectrum of typical vacuum system (Fig.6.1, left).
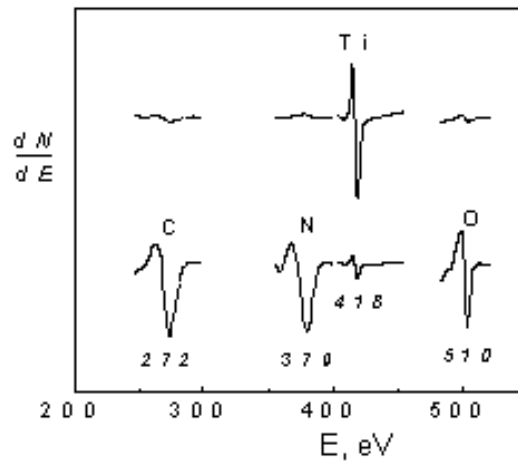
Fig.7.1. Auger-spectrum for "clean" (top) and "dirty" (bottom) surface.

Actually the real surface is oxide covered by adsorbed gases from contaminations of investigated gas (for instance, helium) and residual environment of vacuum system. Both adsorption and chemisorptions take place. As we see at the lower spectrum (Fig.7.1) there are some picks belonged to carbon, nitrogen and oxygen. It is a typical situation as far as any vacuum system has primary hydro carbonic complexes, oxygen, nitrogen and its complexes. All of them participate in formation of surface covering. Hydrogen we cannot see by Auger-electron spectroscopy but it is present in hydrocarbons that are identified as vacuum grease. It explains why such surface is considered as "dirty".

An experience shows that at the first stage of purification procedure some contaminations can be removed rather easily by heating of the sample. But it not concerns oxygen. That is why in our simulations we take oxygen atoms as main component of surface coverage that still is present on the surface even after some purification cycles.

Other way to have guaranteed surface covering is to fill system with pure oxygen when the surface has already completely cleaned by applying special surface purification procedure. As it follows from top spectrum in Fig.7.1 there is only Auger-pick from titanium and nothing else. It's clean surface. Though hydrogen we can not see, it is not present there as it leaves the surface after heating at about 600 K.

The comparison of Auger-spectrum obtained for tungsten wire and titanium vacuum-deposited surface shows that in both cases the surface contamination is consisted of the practically the same atom complexes.

The results of free molecular gas flow rate measurements in channel as a function of oxygen exposition is presented in Fig.7.2.
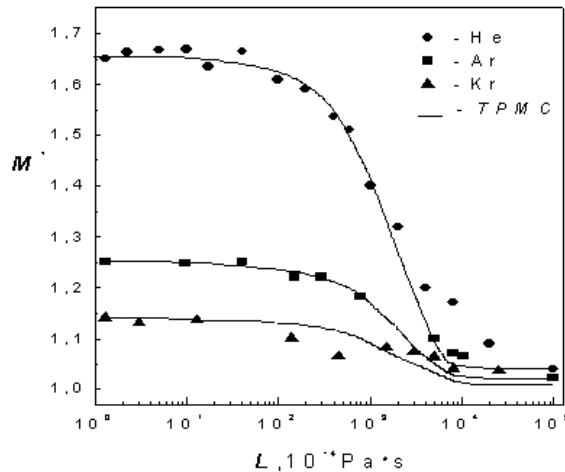
Fig.7.2. Mass flow rate M^* in a cylindrical channel for some noble gases in free molecular regime as a function of oxygen exposition (in Langmuir). Bold line – Test Particle Monte Carlo method (TPMC-simulation).

On the bases of Test Particle method the dependence of gas flow rate on titanium surface coverage with oxygen has been obtained. An original surface stricture is simulated by *hcp* crystal lattice (unlike tungsten surface that is simulated by bcc lattice). The process of gas atom scattering by the surface is simulated similar to the procedure realized in the case of thermal accommodation for *He-W* system. The preliminary results of simulation obtained for free molecular flow rate of *He* in the channel with clean and completely covered by oxygen *Ti* surface are close to experimental results.

Main publications

1. F. D. Polikarpov, A. F. Polikarpov, S. F. Borisov, S. P. Nikulin, and P. V. Tretnikov. Heat Transfer between Tungsten Surface and Glow Discharge Plasmas in Argon and CO_2. Journal of Experimental and Theoretical Physics, 2009, Vol. 109, No. 4, pp. 659–663.
2. A. I. Ukhov, B. T. Porodnov and S. F. Borisov Numerical simulations of gas-dynamic conductivity of microchannels with allowance for their surface structure Journal of Applied Mechanics and Technical Physics Volume 50, Number 5 / September 2009 г. 747-753
3. A.I. Ukhov, B.T. Porodnov, S.F. Borisov. Numerical simulation of roughness of nanochannels and determination of their conductivity // Physical and chemical processes on selection of atoms and molecules and in laser plasma and nanotechnologies: Proc. the XII Jnt. Scien. Conf. - 31 march – 4 apr. 2008. - Zvenigorod. - 2008.
3. A. Ph. Polikarpov, Ph. J. Polikarpov, and S. F. Borisov Energy Exchange between Weakly Ionized Gas and a Metal Surface. AIP Conf. Proc. -- December 31, 2008 -- Volume 1084, pp. 653-658.
5. A. Ukhov, B. Porodnov, and S. Borisov Numerical Simulation of Gas Dynamics Conductivity of Micro Channels with Consideration of Surface Structure. AIP Conf. Proc. -- December 31, 2008 -- Volume 1084, pp. 712-717.

Other publications are in Russian Journals and they will be translated later.